Electronic Supplementary Material (ESI) for ChemComm.

Anion-Induced Formation of Dimers Templated on 2D-Crystals of Cyanostar

Brandon E. Hirsch, Semin Lee, Bo Qiao, Chun-Hsing Chen, Kevin P. McDonald,

Steven L. Tait, Amar H. Flood

Department of Chemistry, Indiana University, 800 East Kirkwood Avenue, Bloomington, IN 47405, USA

S.1 Supplemental STM images

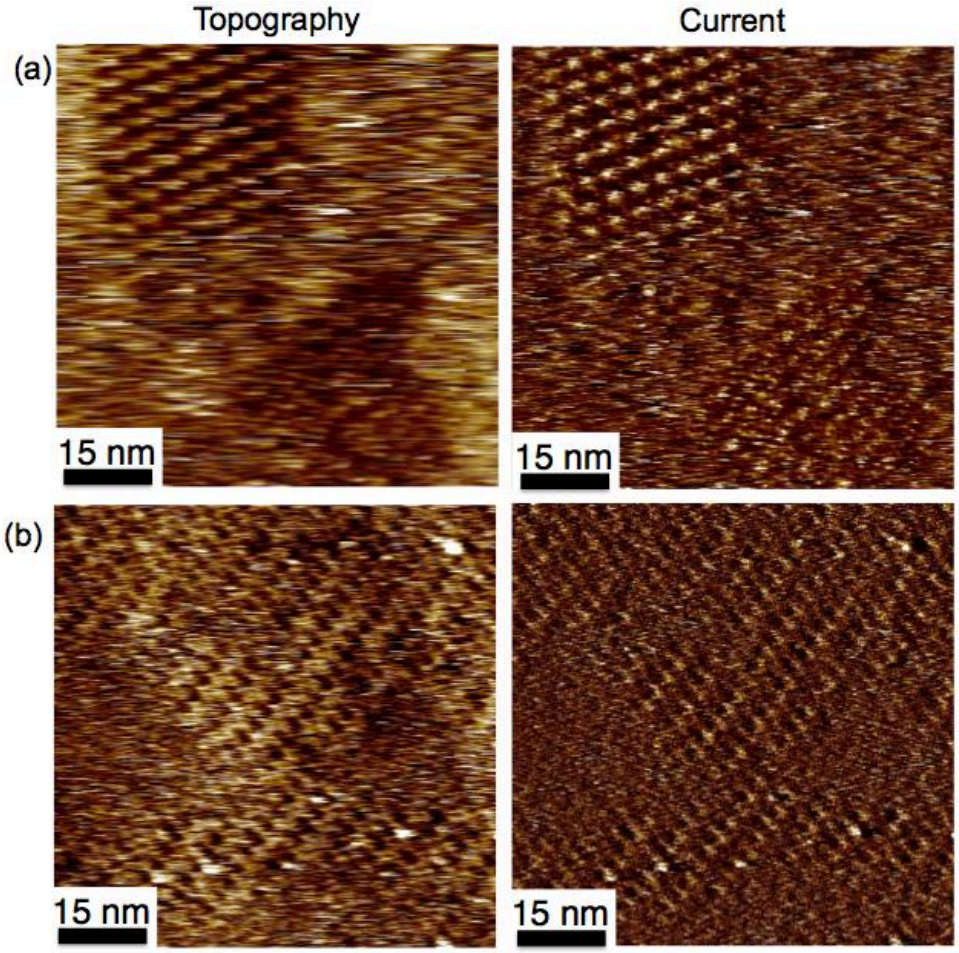

Figure S1. STM topography and current images showing domains of order observed when scanning a solution of **CS-2** (5.0×10^{-6} M^{-1}) at the TCB-HOPG interface. Images recorded with ($T = 23 \pm 0.2$ °C, I_t = (a) 220 pA (b) 10 pA, V_{sub} = (a) –1.1 V, (b) –0.37 V).

Concentrated solutions (50-500 μM) of **CS-2** suffer from larger than ideal background currents that limit scanning conditions. Scanning with 5 μM solutions can be accomplished with a high degree of repeatability (Figure S1).

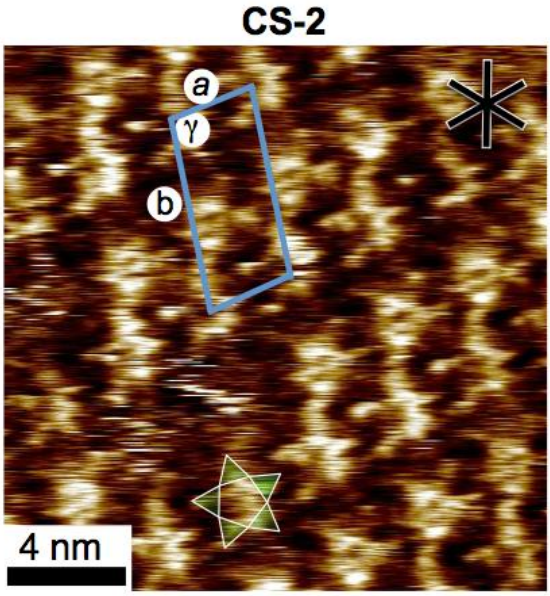

Figure S2. STM topography image of **CS-2** self-assembled on HOPG surface showing the five pointed star appearance along with the two-molecule unit cell of the structure. Image recorded with $T = 23 \pm 0.2$ °C, $I_t = 10$ pA, $V_{sub} = -0.58$ V.

S.2 2D Crystal Packing Model Analysis

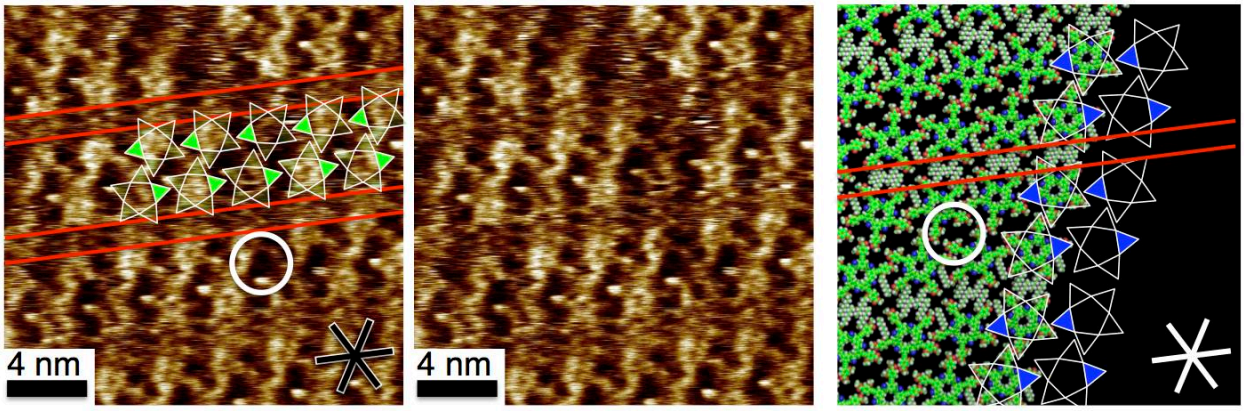

Figure S3. STM topography image showing the *anti*-parallel rows of pentamers of the 2D crystal observed when scanning a solution of **CS-2** (5.0×10^{-6} M^{-1}) at the TCB-HOPG interface. The red lines demarcate the lower contrast features which are channels of adsorbed alkyl chains believed to be aligned along a major axis of HOPG. Image recorded with $T = 23 \pm 0.2$ °C, $I_t = 10$ pA, $V_{sub} = -0.58$ V. The white circle highlights one of the bare regions of the surface between the molecules of the double row. The packing model demonstrates the *anti*-parallel double rows of pentamers with three alkyl chains adsorbed onto the surface, two of which interdigitate in the rows indicated by the red lines. The angle of the chains is not unambiguously resolved in the STM images, but may allow the chains to align along the low index directions of graphite, as is often observed for alkyl groups on HOPG.

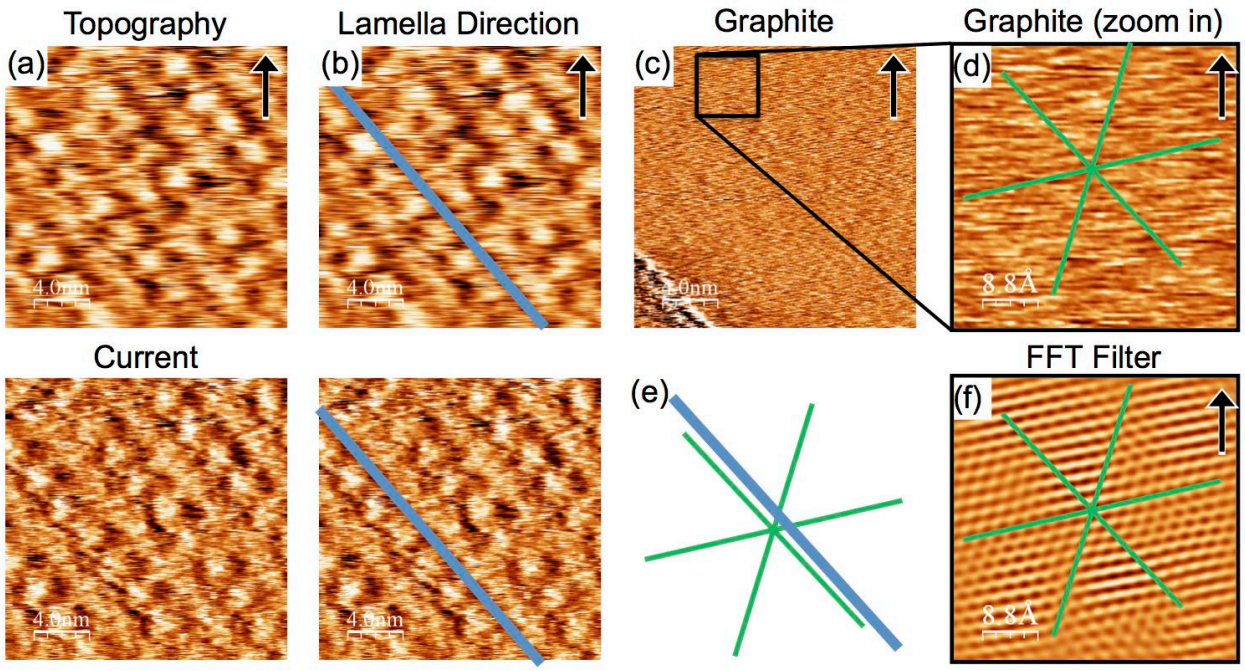

Figure S4. STM analysis showing the alignment of the lamella rows with a major axis of graphite. STM images (a) topography and current of the **CS-2** self-assembly on HOPG. (b) Assignment of the lamella directions. (c) HOPG lattice acquired immediately after the acquisition of the images in (a). (d) Zoom-in region of the graphite lattice and assignment of the major axes. (e) comparison of lamella direction to the HOPG lattice directions. (f) FFT filtered image of (d) and verification of lattice assignment. Images recorded with (T = 23 ± 0.2 °C, I_t = (a) 120 pA (b) 400 pA, V_{sub} = (a) –0.202 V, (b) –0.002 V). Close attention was paid to ensure that the correction factors obtained from the graphite lattice were applied to **CS-2** images with the same scan speed, size, and slow scan direction. The slow scan direction is indicated in the images with a black arrow that appear in the upper right of each image. In addition the graphite correction data was always obtained within 5 minutes of imaging the **CS-2** monolayer**.**

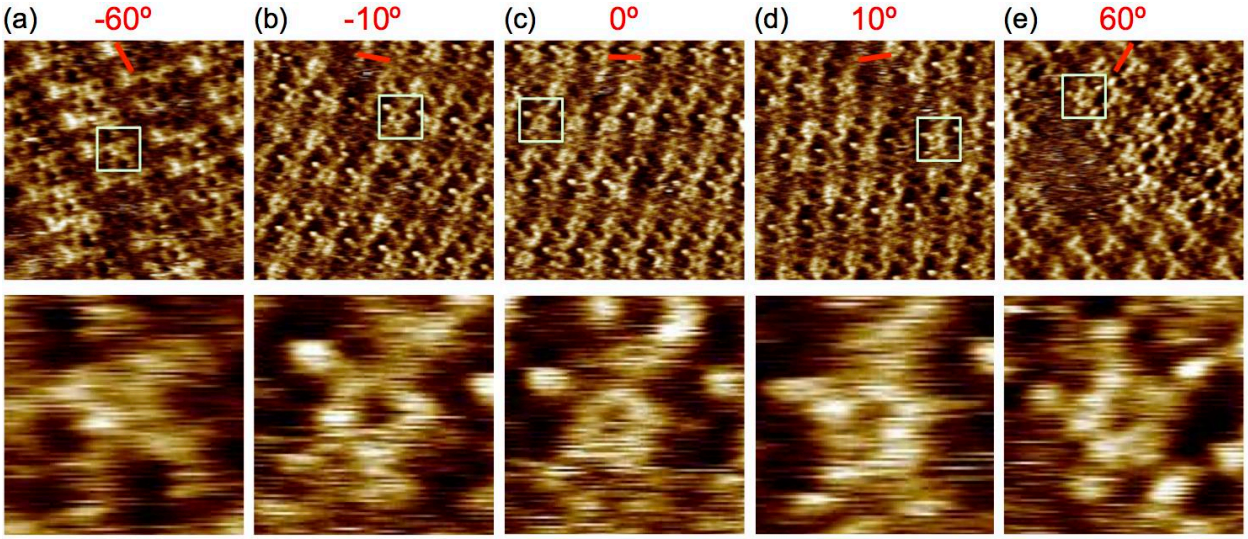

Figure S5. STM rotational analysis (a-e) of **CS-2** monolayer structure with insets representing best resolution of the star shape. The rotation angle (scan direction relative to lamella direction) is represented by red line and related red number. The appearance of the "star" shape and its central cavity changes as the image is rotated. In the final image (e) the **CS-2** molecule appears as one of the clearest stars with its central cavity well resolved. Images recorded with T = 23 ± 0.2 °C, I_t = 10 pA, V_{sub} = –0.58 V.

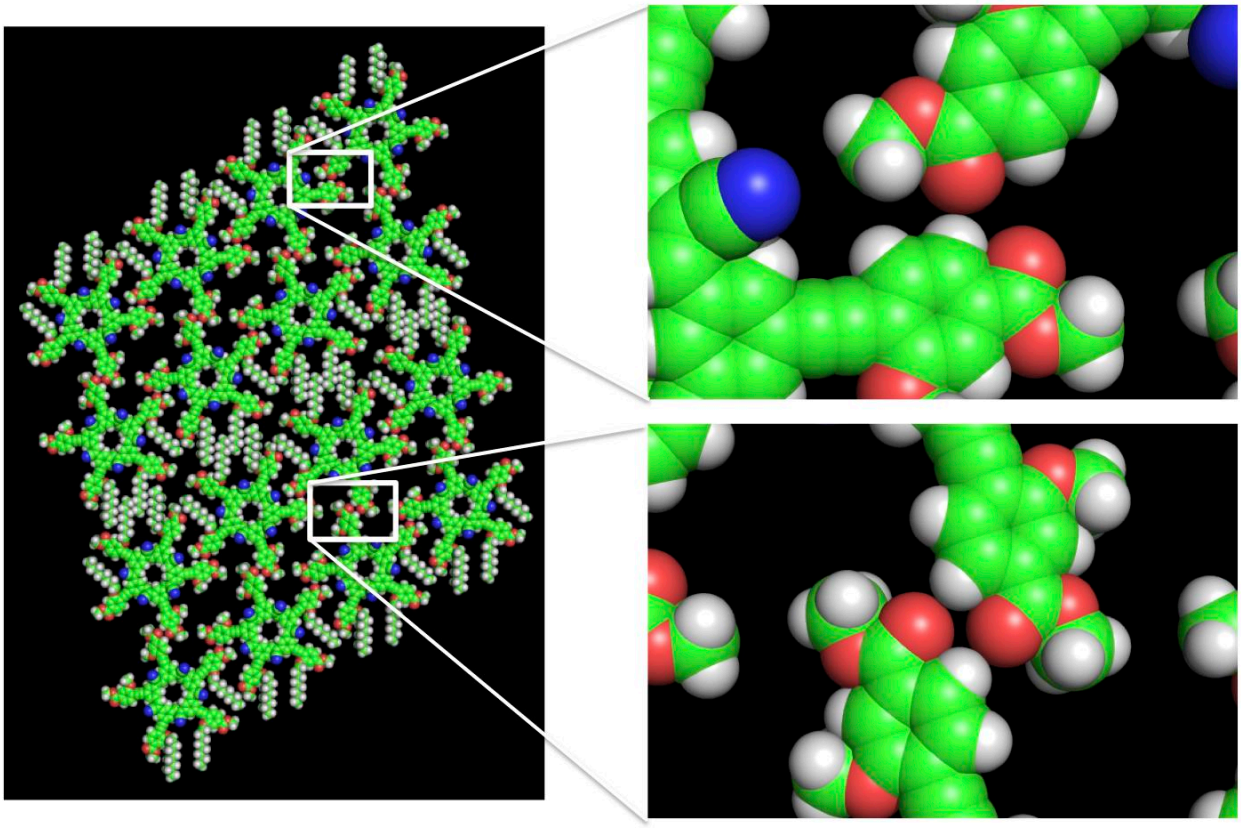

Figure S6. Packing model of **CS-2** self-assembly on HOPG derived from STM measurements and the molecule geometry (as discussed below). Insets highlight the ester contacts in this model that would help stabilize the 2D crystal.

Solving and Refining 2D Crystal Structures using Molecular Replacement

The tentative packing model for the **CS-2** monolayer on HOPG (Figs. 1f and S6) was constructed using a self-consistent strategy that is reminiscent of molecular replacement methods typically used with the structure refinement of low-resolution X-ray crystal data obtained from single crystals of biomolecules.[1S1] In contrast to electron density maps from X-ray crystallography, real-space STM imaging generates a "topography" map which is actually a record of STM tip height as it scans across the surface with constant tunneling current, *i.e.*, a convolution of surface topography and the local density of electronic states near the Fermi level. An error signal images (deviation of actual tunneling current from constant setpoint value) is usually recorded and analyzed also, often being more sensitive to sharp changes in surface features than the topography.

The workflow used herein involves (1) measuring periodic unit cell distances from the repeating pattern present in the STM image, (2) representing the molecules as shapes of the right size (stars, in the present case) and then placing these on lattice positions within the unit cell. (3) Using the contrast present in the STM images the orientations are optimized while maintaining non-overlapping shapes to generate an initial solution to the crystal structure (akin to shape tessellation). Subsequently, (4) an overlay of the structural model of the molecules (in place of the shapes) onto the STM image helps identify the chemical

character (attractive and repulsive) of the possible intermolecular contacts. Finally, (5) the packing is optimized (using bond and dihedral rotations) to match all the STM unit cell data (STM images generated with different scan conditions and tip configurations). Refinement involves iterating steps 4 and 5.

Tip convolution effects are a concern in shape analysis of STM data, since the actual shape, size and configuration of the tip are usually uncharacterized. Therefore, periodic spacing data are the most reliable measurements from the corrected STM images. However, after the model has been constructed to match the periodicity of the image, further insight can often be gained from the STM data by analyzing local features and shapes. These allow further refinement of the packing models (steps 4 and 5 above) that go beyond the structural characterization that could be achieved by surface diffraction studies. For example, in the system studied here, this analysis leads to insight into the possible ester contacts (Fig S6) that may contribute significantly to the ordering and stability of the **CS-2** monolayer on HOPG. In this way, STM image analysis can be used to take full advantage of the real space imaging information.

S.3 Dimer Model Analysis

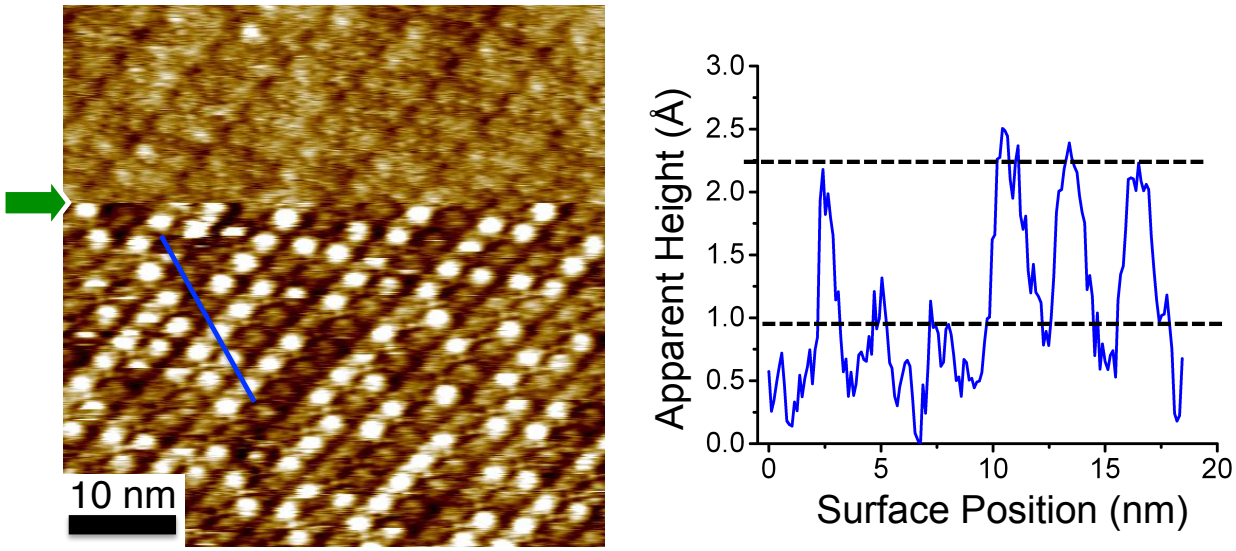

Figure S7. STM topography image showing the bright contrast features attributed to anion induced dimer formation around PF_6^- along with the apparent height profile showing the features rising on average 1.4 Å above the monolayer **CS-2** receptors. Image recorded with T = 23 ± 0.2 °C, I_t = 100 pA, V_{sub} = –0.7 V.

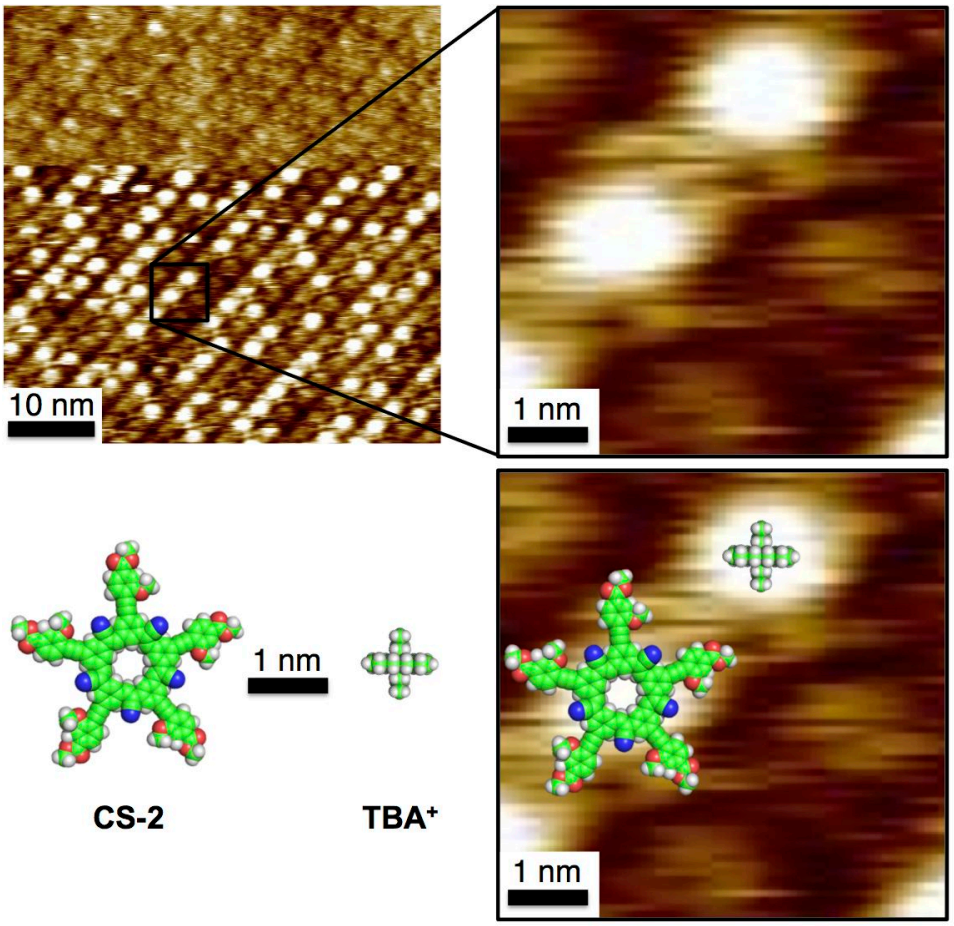

Figure S8. STM analysis on the size of the bright features compared to scaled space-fill models of a **CS-2** molecule and the TBA^+ counter-cation. From the overlaid models on the STM image it becomes clear that the TBA^+ counter-cation is too small to give rise to the observed bright features. In addition to this size explanation, anion additions at low equivalents (< 0.01 eq) are known from prior work to produce the 2:1 dimer species.[22]

S.4 Electric Field and Solvent Sensitivity

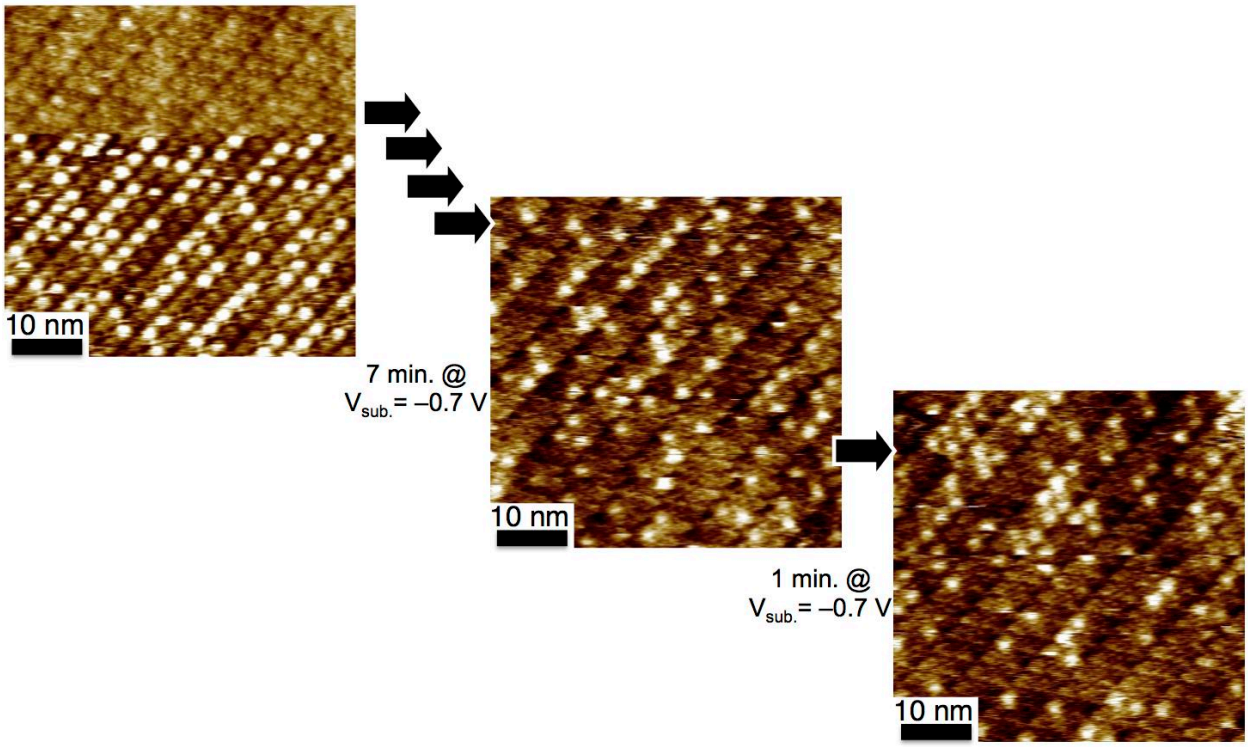

Figure S9. STM topography image sequence showing the decrease in the number of bright contrast features attributed to anion induced dimer formation around PF_6^- as the system is scanned with a negative substrate bias. Images are recorded with T = 23 ± 0.2 °C, I_t = 100 pA, V_{sub} = –0.7 V.

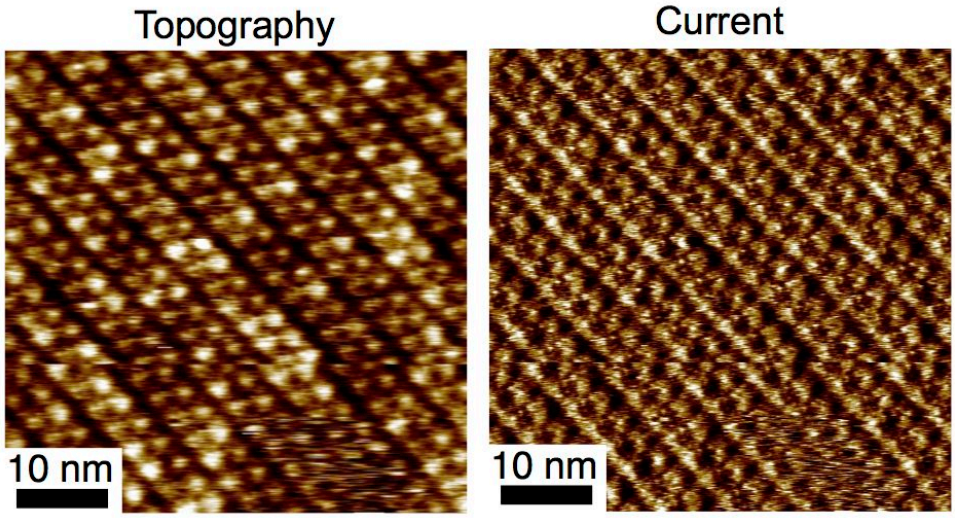

Figure S10. Representative STM image obtained during one of the other nine experimental replicates examining the self-assembly at the solution-graphite interface in the presence of anions. Height contrast is observed and assigned as dimers from **CS-2$_2$•PF$_6^-$** on the surface of HOPG. Images were recorded with T = 23 ± 0.2 °C, I_t = 90 pA V_{sub} = –0.9 V.

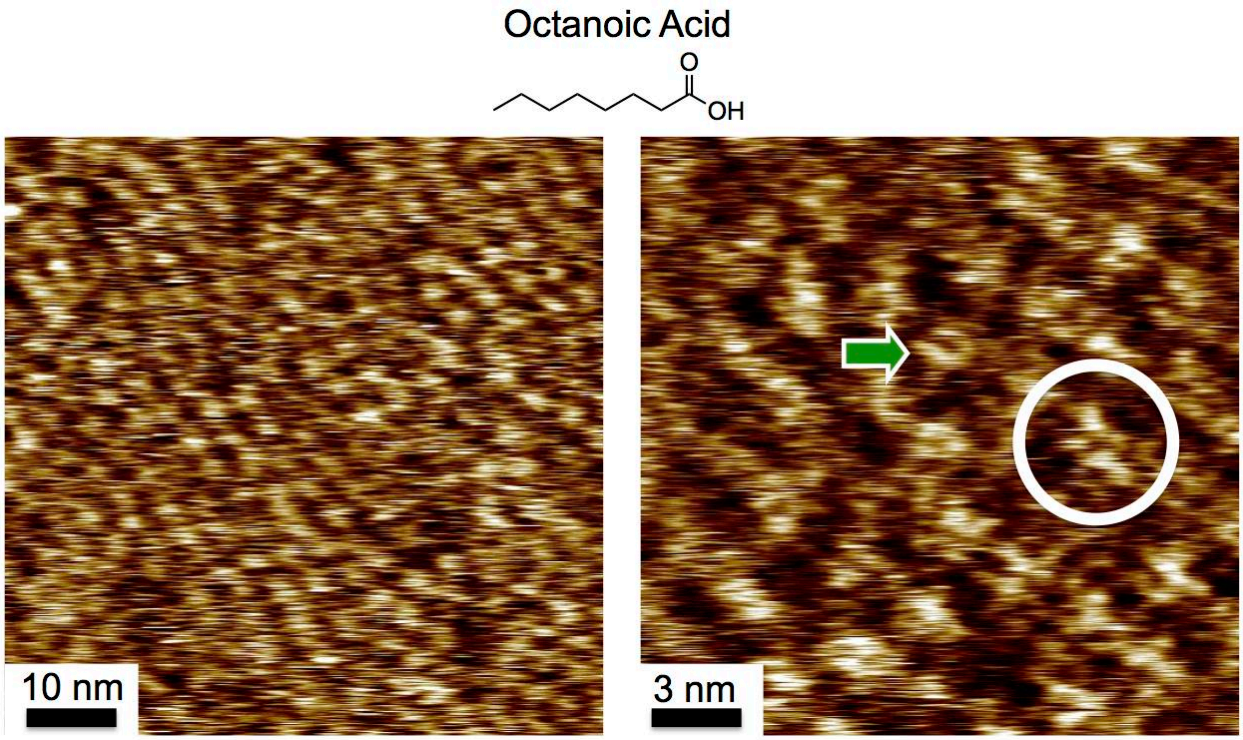

Figure S11. STM topography image showing the emergence of short-range order observed when scanning at the octanoic acid-HOPG interface. The white circle surrounds a single star-shape **CS-2** molecule. The green arrow marks the resolution of the cavity inside one of the **CS-2** molecules. [**CS**] = 1.2×10^{-4} M^{-1}. Images recorded with T = 23 ± 0.2 °C, I_t = 30 pA, V_{sub} = –0.3 V.

S.5 X-ray Crystallography

Single crystals of **CS-1**$_2$•ClO_4^-•TEA^+ were grown by slow evaporation of a solution of dichloromethane and ethanol (1:1). The sample was investigated with synchrotron radiation at the ChemMatCARS beamline, Advanced Photon Source, Argonne National Laboratory, Chicago, utilizing the SCrAPS program (http://www.iumsc.indiana.edu/projects/SCrAPS/index.html). A colorless crystal (approximate dimensions 0.030 × 0.025 × 0.010 mm^3) was placed onto the tip of a glass capillary and mounted on an Apex Kappa Duo diffractometer and measured at 100 K. The data collection was carried out using synchrotron radiation (λ = 0.41328, silicon 111 and 311 monochromators, two mirrors to exclude higher harmonics) with a frame time of 1 second and a detector distance of 6.0 cm. A randomly oriented region of reciprocal space was surveyed to the extent of hemispheres. Two major sections of frames were collected with 0.50º steps in ϕ and a detector position of –5° in 2θ. Data to a resolution of 0.84 Å were considered in the reduction. Final cell constants were calculated from the xyz centroids of 9892 strong reflections from the actual data collection after integration (SAINT).[S3] The intensity data were corrected for absorption (SADABS).[S4] Please refer to Table 1 for additional crystal and refinement information.

Structure solution and refinement

The space group P–1 was determined based on intensity statistics and lack of systematic absences. The structure was solved using SIR-92[S5] and refined (full-matrix-least squares) using the Oxford University Crystals for Windows system.[S6] A direct-methods solution was calculated, which provided most non-hydrogen atoms from the E-map. Full-matrix least squares / difference Fourier cycles were performed, which located the remaining non-hydrogen atoms.

The asymmetric unit of structure **CS-1**$_2$•ClO_4^-•TEA^+ contains one cyanostar macrocycle, two dichloromethane solvent molecules, half of the perchlorate anion with the chlorine atom located at the special position (½, 0, ½), and half of the tetraethylammonium cation located on the special position with the cation's nitrogen atom at (½, 0, 0). Structure **CS-1**$_2$•ClO_4^-•TEA^+ exhibits whole molecule disorder. The disorders present in the macrocycle and in the bound perchlorate anion were modeled successfully.

The two-part disorder on the macrocycle was modeled such that the occupancies of the major and minor components sum to 1, each corresponds to 60% *M* and 40% *P* stereoisomers. Disorder in the anion at the special position was modeled with occupancies of the major (0.312(6) ≡ 62%) and minor (0.188(6) ≡ 37%) components sum to 0.5. The other half of the anion is located at the symmetry-related position in the unit cell.

Disorder modeling for dichloromethane and tetraethylammonium proved to be problematic on account of the fact that, while the approximate locations of the two dichloromethane solvent molecules and the tetraethylammonium cation were certain and in close proximity to each other, the two disordered molecules of dichloromethane occupy a sizable volume. Challenges in refining the disordered dichloromethane directly affected the refinement of the tetraethylammonium cation, which itself shows less disorder but it comprised of much

lighter atoms. Consequently, Platon SQUEEZE[S7] was implemented and showed an electron count of 142 e^- corresponding to two dichloromethane molecules and one tetraethylammonium cation. The associated volume of 649 $Å^3$ represents a space that is equivalent to 8 solvent molecules and one tetraethylammonium cation, thus, there is some void space on average.

Both the ordered non-hydrogen atoms and the major component of the disordered non-hydrogen atoms were refined with anisotropic displacement parameters, and the minor component of the disordered non-hydrogen atoms was refined isotropically. The hydrogen atoms were placed in ideal positions and refined as riding atoms. The final full matrix least squares refinement converged to R1 = 0.1546 and wR2 = 0.4455 (F^2, all data).

Table S1. Crystal data and structure refinement for **CS-1**$_2$•ClO_4^-•TEA^+.

Empirical formula	$C_{130}\ H_{130}\ Cl_1\ N_{10}\ O_4$	
Formula weight	1931.98	
Crystal color, shape, size	colorless plate, 0.030 × 0.025 × 0.010 mm^3	
Temperature	100 K	
Wavelength	0.41328 Å	
Crystal system, space group	Triclinic, P –1	
Unit cell dimensions	a = 14.1468(13) Å	α= 103.7800(10)°.
	b = 14.5133(13) Å	β= 102.6190(10)°.
	c = 16.7542(15) Å	γ = 99.9070(10)°.
Volume	3167.8(5) $Å^3$	
Z	1	
Density (calculated)	1.013 Mg/m^3	
Absorption coefficient	0.081 mm^{-1}	
F(000)	1028.998	
Data collection		
Diffractometer	Bruker Apex Kappa Duo, Bruker	
Theta range for data collection	0.864 to 16.151°.	
Index ranges	$-19 \le h \le 18$, $-19 \le k \le 18$, $0 \le l \le 22$	
Reflections collected	15279	
Independent reflections	15279 [R(int) = 0.032]	
Observed Reflections	10461	
Completeness to theta = 14.536°	94.8 %	
Solution and Refinement		
Absorption correction	Semi-empirical from equivalents	
Max. and min. transmission	1.00 and 1.00	
Solution	Direct methods	
Refinement method	Full-matrix least-squares on F^2	
Weighting scheme	$w = w' \times [1 - (\sigma(F)/6\sigma(Fest))^2]^2$, with	
	$w' = (P_0T_0'(x) + P_1T_1'(x) + \ldots + Pn\text{-}_1Tn\text{-}_1')^{-1}$	
Data / restraints / parameters	15259 / 1055 / 958	
Goodness-of-fit on F^2	1.0542	
Final R indices [I>2sigma(I)]	R1 = 0.1546, wR2 = 0.3955	
R indices (all data)	R1 = 0.1806, wR2 = 0.4455	
Largest diff. peak and hole	0.99 and –1.04 e.$Å^{-3}$	

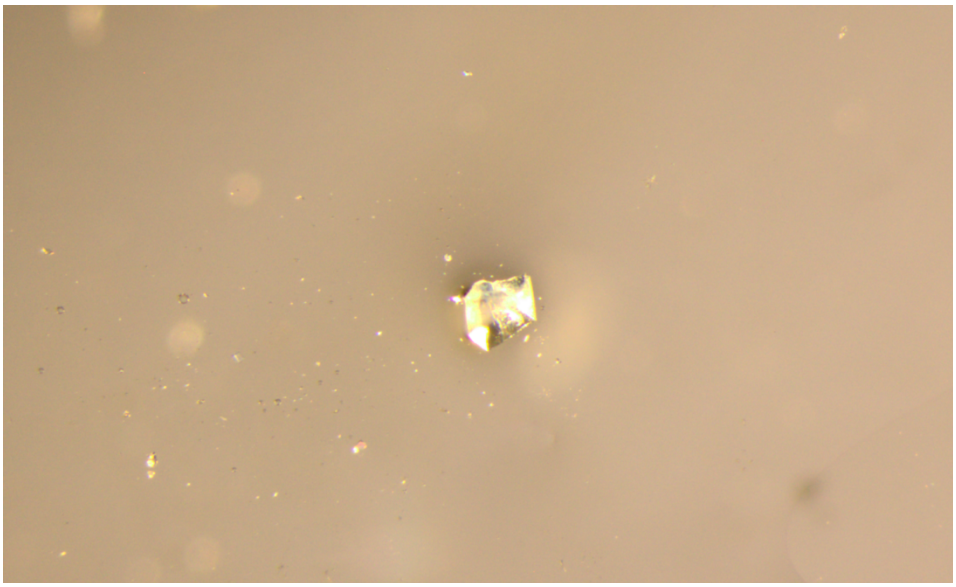

Figure S12. Photograph of the single crystal of **CS-1**$_2$•ClO_4^-•TEA^+ used for the X-ray crystallography study.

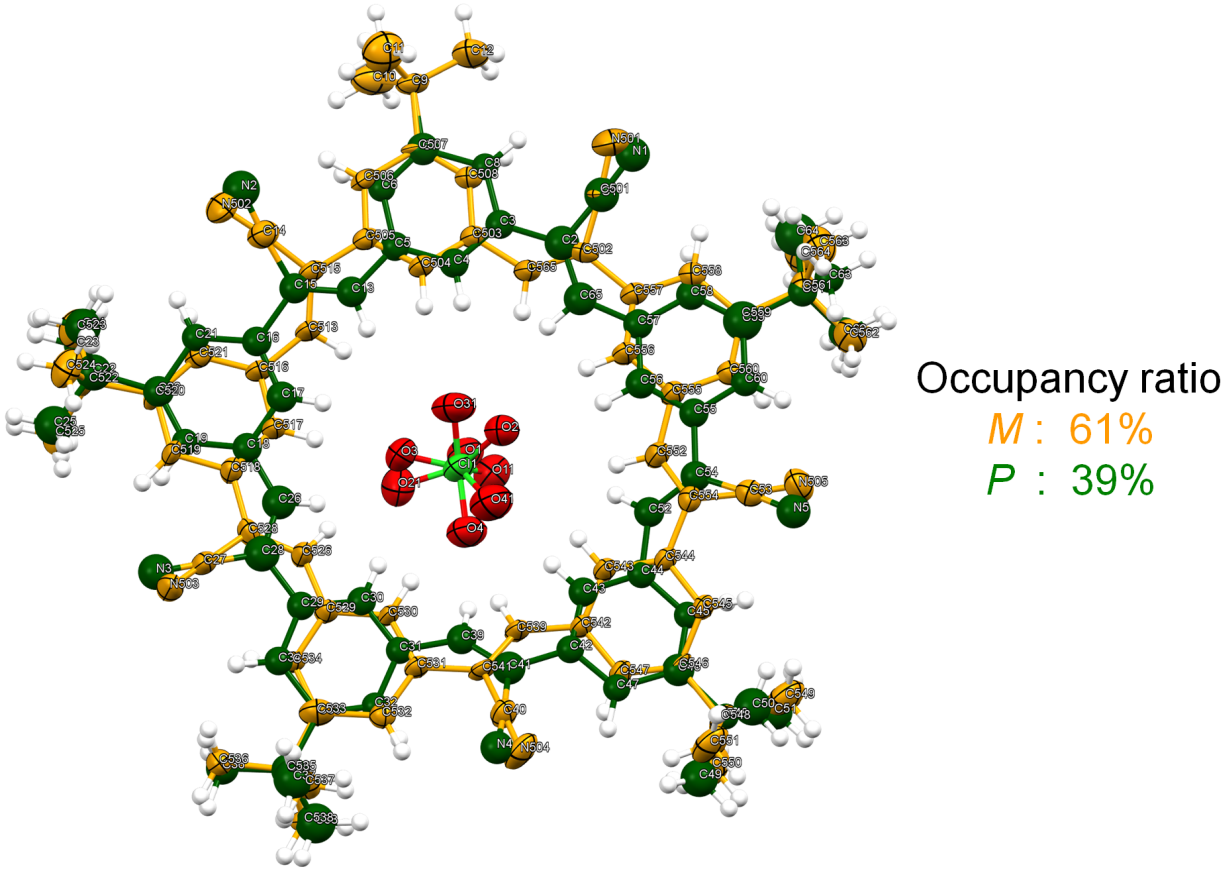

Figure S13. Asymmetric unit of **CS-1**$_2$•ClO_4^-•TEA^+ (ellipsoids drawn in 50% probability).

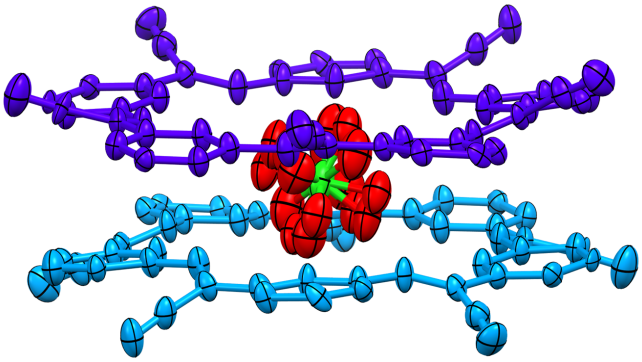

Figure S14. A 2:1 sandwich complex of **CS-1**$_2$•ClO_4^- exhibiting the bowl-like curvature of **CS-1** (methyl groups and hydrogen atoms are omitted for clarity; the top and bottom cyanostars are colored purple and cyan, respectively).

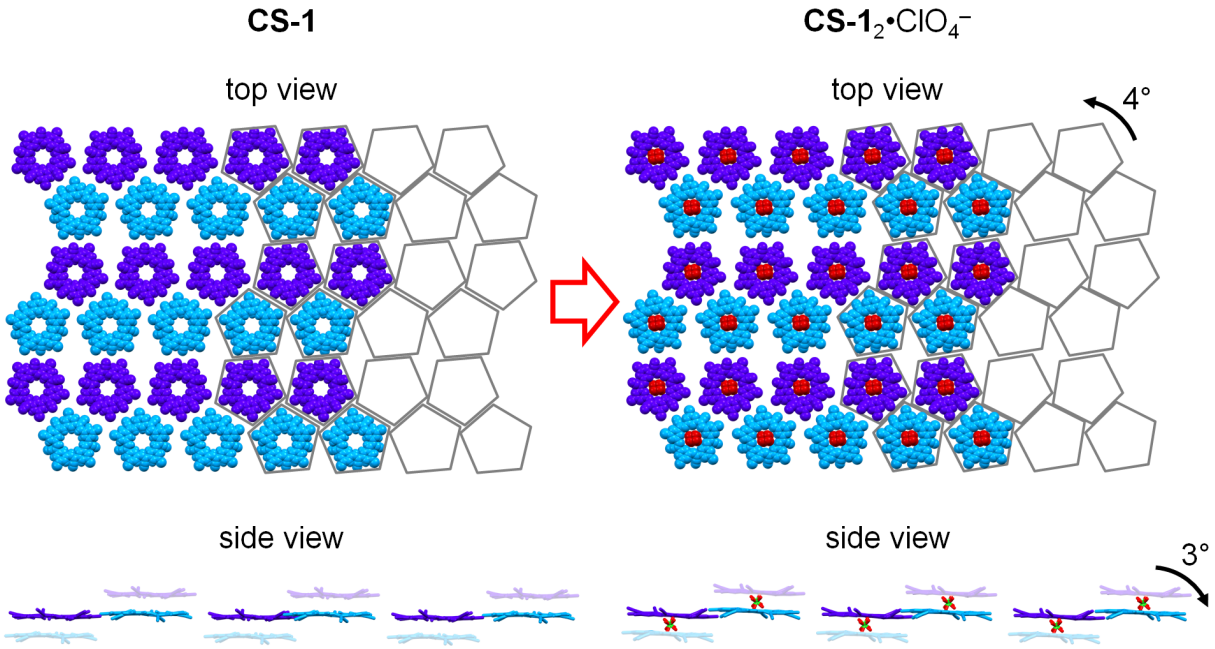

Figure S15. 2D Dürer tiling of **CS-1** and **CS-1**$_2$•ClO_4^-•TEA^+ (methyl groups and hydrogen atoms are omitted for clarity). The 4º relates to in-plane rotation with respect to the structure if **CS-1** alone while the 3º is an out-of-plane rotation (the top and bottom cyanostars are colored purple and cyan, respectively).

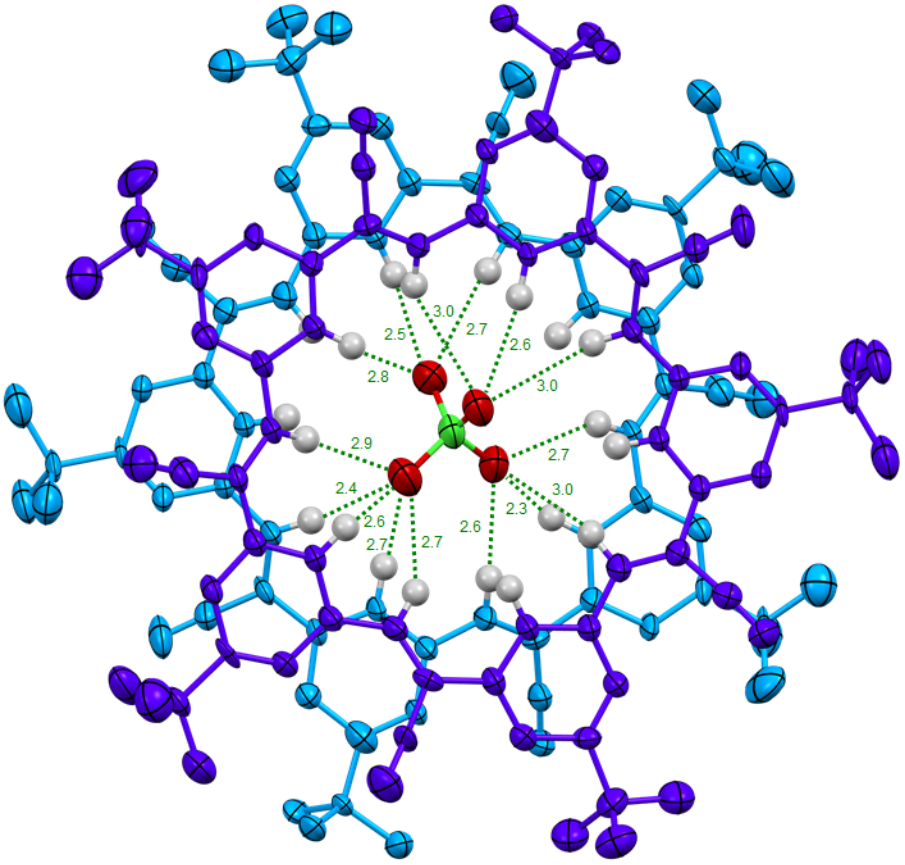

Figure S16. CH•••O hydrogen bond interactions ($d \leq 3$ Å, green dotted lines, distances labeled in angstroms) within the **CS-1**$_2$•ClO_4 complex (one set of disordered ClO_4^- is visualized for clarity; the top and bottom cyanostars are colored purple and cyan, respectively).

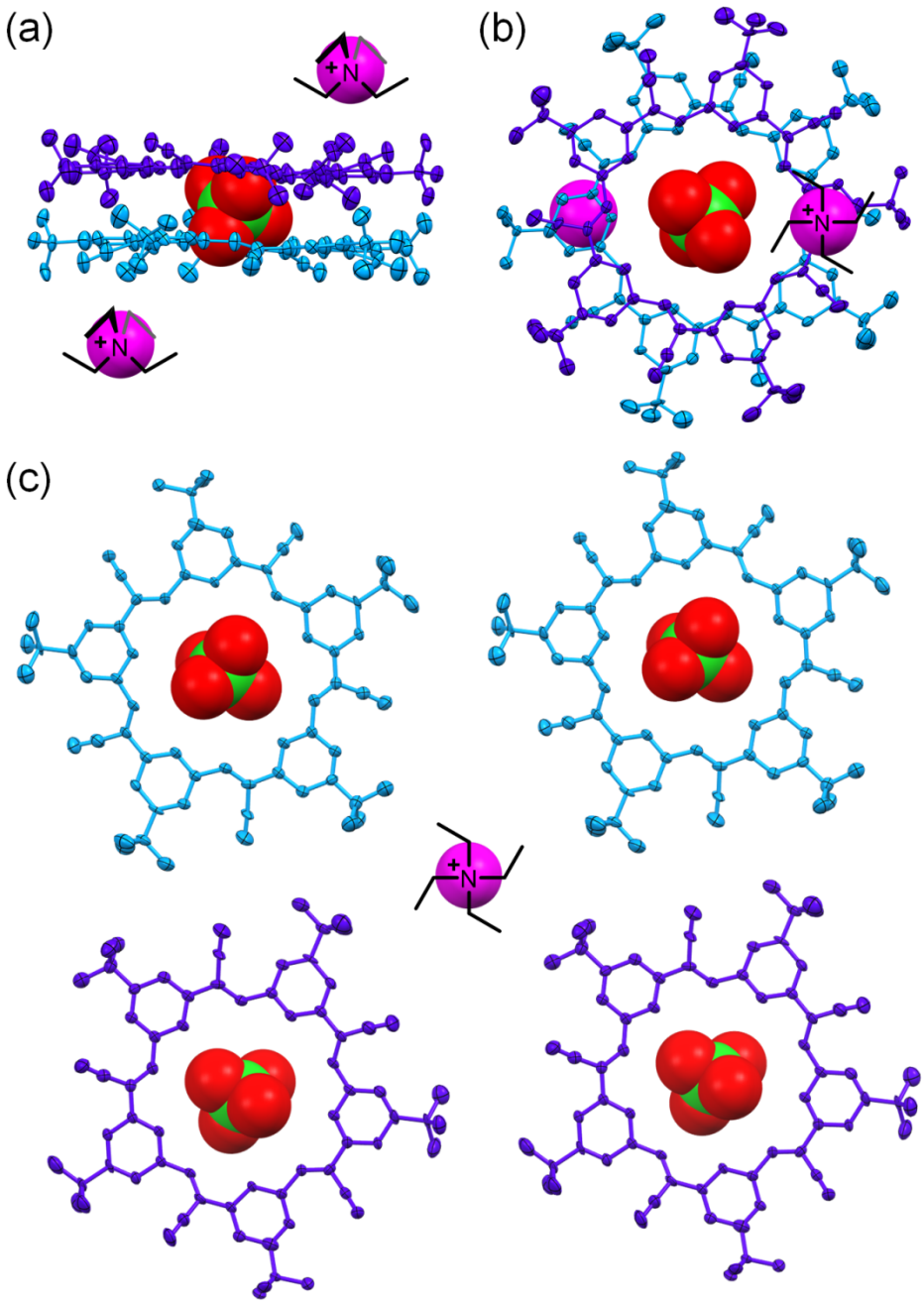

Figure S17. Representations showing the position of the counter cation. Position of the nitrogen atom (magenta) in the tetraethylammonium cation shown relative to the $\mathbf{CS_2}$•ClO_4^- complex (a) side view and (b) top view and (c) within the 2D Dürer tiling (before the implementation of SQUEEZE). The nitrogen atom was located during XRD structure refinement. However, the positions of the ethyl chains were not resolved on account of significant disorder present in the adjacent solvent molecules (not shown). See refinement above for more details.

S.6 General Methods of Syntheses

All reagents were obtained from commercial suppliers and used as received unless otherwise noted. 2-(3-(Hydroxymethyl)-5-iodophenyl)acetonitrile was prepared from (5-iodo-1,3-phenylene)dimethanol.[S8] Column chromatography was performed on silica gel (160 – 200 mesh, Sorbtech), and thin-layer chromatography (TLC) was performed on precoated silica gel plates (0.25 mm thick, Silicycle) and observed under UV light. Nuclear magnetic resonance (NMR) spectra were recorded on Varian Inova (400 MHz and 500 MHz) and Varian VXR (400 MHz) at room temperature (298 K). Chemical shifts were referenced on tetramethylsilane (TMS) or residual solvent peaks. High resolution electrospray ionization (ESI) and chemical ionization (CI) mass spectrometry was performed on a Thermo Electron Corporation MAT 95XP-Trap mass spectrometer.

S.7 Syntheses and Characterization of Compounds

List of abbreviations

THF	tetrahydrofuran
MeCN	acetonitrile
PCC	pyridinium chlorochromate

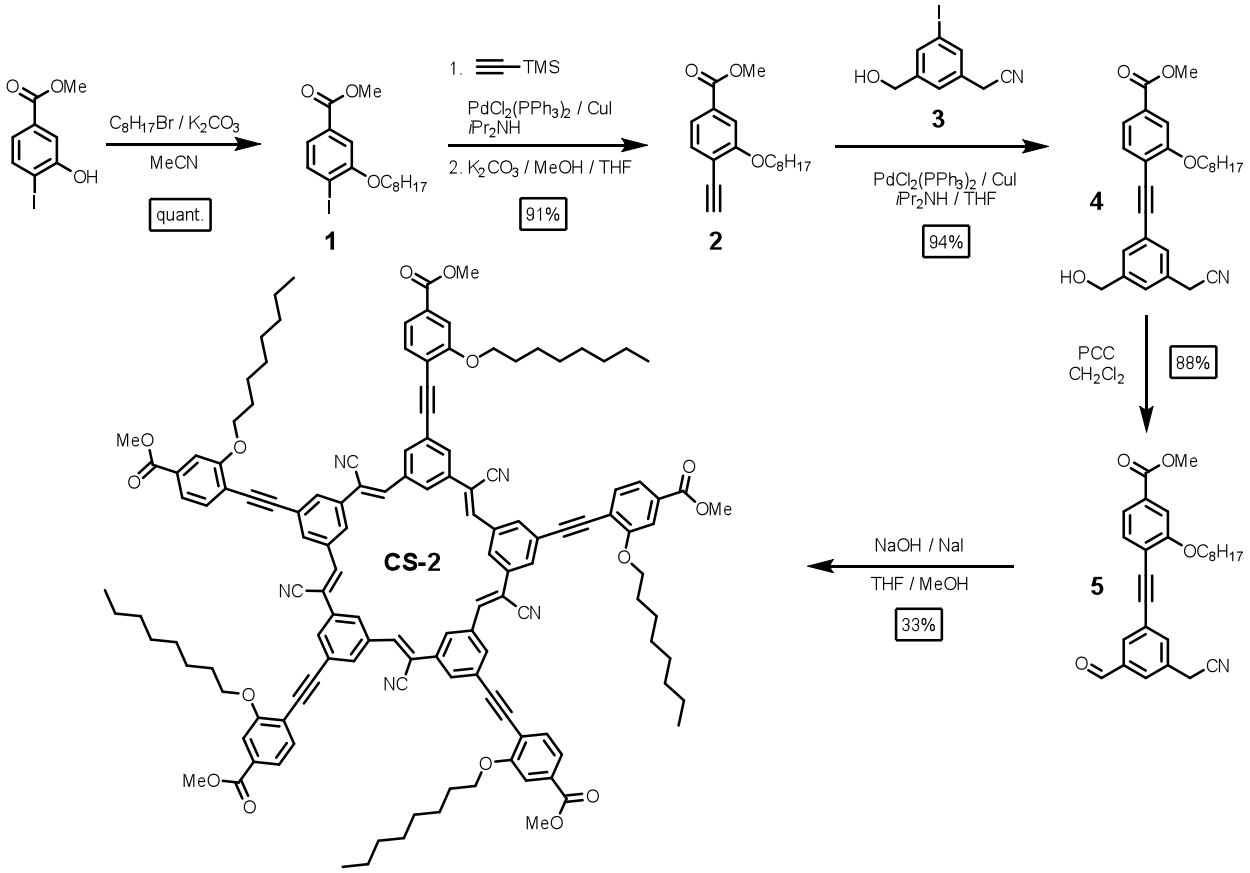

Scheme S1. Synthesis of **CS-2**.

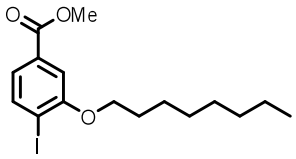

Methyl 4-iodo-3-(octyloxy)benzoate (1): A mixture of methyl 3-hydroxy-4-iodobenzoate[S9] (2 g, 7.19 mmol), 1-bromooctane (1.53 g, 7.9 mmol), K_2CO_3 (2 g, 14.4 mmol) and KI (120 mg, 0.72 mmol) in MeCN (100 mL) was refluxed for 5 h. MeCN was removed in vacuo, extracted with EtOAc, washed with brine, dried with $MgSO_4$ and concentrated in vacuo. Column chromatography on silica gel with hexane:EtOAc = 9:1 resulted in a white solid product (2.81 g, 7.2 mmol, quantitative yield). ^{1}H NMR (400 MHz, $CDCl_3$) δ = 7.84 (d, J = 8.2 Hz, 1H), 7.41 (s, 1H, 7.35 (d, J = 7.8 Hz, 1H), 4.07 (t, J = 6.3 Hz, 2H), 3.91 (s, 3H), 1.85 (m, 2H), 1.53 (m, 2H), 1.30 (m, 8H), 0.89 (t, J = 6.6 Hz, 3H). ^{13}C NMR (100 MHz, $CDCl_3$) δ = 165.9, 157.3, 138.9, 131.0, 122.6, 111.6, 93.0, 69.0, 51.9, 31.5, 28.97, 28.94, 28.7, 25.8, 22.4, 13.8. HRMS-CI: $C_{16}H_{23}IO_3$ $[M]^+$, Calculated: 390.0686, Found: 390.0692.

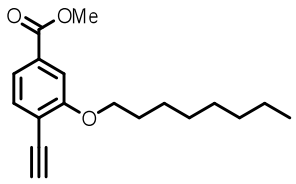

Methyl 4-ethynyl-3-(octyloxy)benzoate (2): A solution of methyl 4-iodo-3-(octyloxy)benzoate (1.33 g, 3.41 mmol) and diisopropylamine (2 mL, 13.6 mmol) in THF (50 mL) was degassed with argon for 20 min. $PdCl_2(PPh_3)_2$ (47 mg, 0.068 mmol), CuI (32 mg, 0.17 mmol) and trimethylsilylacetylene (0.8 mL, 5.6 mmol) were added and stirred under an argon atmosphere for 5 h. The reaction mixture was filtered and the solvent was removed in vacuo. Column chromatography on silica gel with hexane:EtOAc = 9:1 produced **2** as a brown oil (1.24 g, 3.4 mmol, quantitative yield). This intermediate methyl 3-(octadecyloxy)-4-((trimethylsilyl)ethynyl)benzoate (600 mg, 1.66 mmol) was dissolved in MeOH (20 mL) and a saturated solution of K_2CO_3 in MeOH (2 mL) was added and stirred for 2 h. The solvent was removed in vacuo and the resulting crude mixture was suspended in CH_2Cl_2 and filtered through a pad of Celite to give a brown oil product **2** (435 mg, 1.51 mmol, 91% yield). ^{1}H NMR (400 MHz, $CDCl_3$) δ = 7.57 (dd, J = 7.8, 1.2 Hz, 1H), 7.53 (d, J = 1.2 Hz, 1H), 7.49 (d, J = 7.8 Hz, 1H), 4.09 (t, J = 6.6 Hz, 2H), 3.92 (s, 3H), 3.39 (s, 1H), 1.85 (m, 2H), 1.50 (m, 2H), 1.29 (m, 8H), 0.89 (t, J = 7.0 Hz, 3H). ^{13}C NMR (100 MHz, $CDCl_3$) δ = 166.4, 160.0, 133.7, 131.3, 121.2, 116.3, 112.3, 83.6, 79.3, 68.9, 52.2, 31.7, 29.2, 29.1, 28.9, 25.8, 22.6, 14.0. HRMS-CI: $C_{18}H_{24}O_3$ $[M]^+$, Calculated: 288.1720, Found: 288.1709.

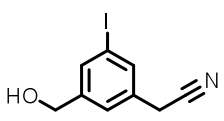

2-(3-(Hydroxymethyl)-5-iodophenyl)acetonitrile (3): (5-Iodo-1,3-phenylene)dimethanol[S8] (5 g, 18.9 mmol) was dissolved in toluene (200 mL) and heated to 90 °C on an oil bath. The solution was cooled to 70°C and 47–

49% aqueous solution of HBr (2.8 mL, 24.6 mol) was added and stirred for 3 h. The reaction mixture was cooled using an ice bath and neutralized with Na_2CO_3 solution. The organic phase was collected and the aqueous layer was further extracted with EtOAc. Organic layers were combined and dried with $MgSO_4$, filtered then concentrated under vacuum. The resulting crude oil product was dissolved in THF (50 mL), MeOH (20 mL) and water (50 mL). KCN (1.6 g, 24.6 mmol) was added and stirred at 80 °C for 8 h. After cooling to room temperature, THF and MeOH were removed in vacuo. The mixture was extracted with EtOAc and the organic phase was dried with $MgSO_4$, filtered and the solvents were removed in vacuo. Column chromatography on silica gel with hexane:EtOAc = 1:1 to 1:2 resulted in a white solid product (4.3 g, 15.7 mmol, 84% yield). ^{1}H NMR (400 MHz, $CDCl_3$) δ = 7.67 (s, 1H), 7.57 (s, 1H), 7.29 (s, 1H), 4.65 (d, J = 4.7 Hz, 2H), 3.70 (s, 2H), 2.29 (t, J = 4.8 Hz, 1H). ^{13}C NMR (100 MHz, $CDCl_3$) δ = 144.0, 135.4, 135.1, 131.8, 125.3, 117.27, 94.6, 63.2, 22.8. HRMS-ESI: C_9H_7INO $[M - H]^-$,Calculated: 271.9567, Found: 271.9568.

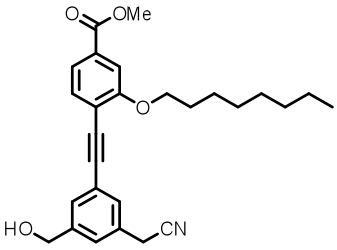

Methyl 4-((3-(cyanomethyl)-5-(hydroxymethyl)phenyl)ethynyl)-3-(octyloxy)benzoate (4): A solution of methyl 4-ethynyl-3-(octyloxy)benzoate (1 g, 3.47 mmol), 2-(3-(hydroxymethyl)-5-iodophenyl)acetonitrile and diisopropylamine (0.7 mL, 4.8 mmol) in THF (50 mL) was degassed with argon for 20 min. $PdCl_2(PPh_3)_2$ (17 mg, 0.024 mmol) and CuI (12 mg, 0.06 mmol) was added and stirred at 70 °C for 5 h. After cooling to room temperature, the reaction mixture was filtered and the solvent was removed in vacuo. Column chromatography on silica gel with CH_2Cl_2:EtOAc = 9:1 resulted in a white solid product (1.28 g, 2.95 mmol, 94% yield). ^{1}H NMR (400 MHz, $CDCl_3$) δ = 7.61 (d, J = 7.8 Hz, 1H), 7.55 (s, 1H), 7.52 (d, J = 8.0 Hz, 1H), 7.50 (s, 1H), 7.43 (s, 1H), 7.35 (s, 1H), 4.73 (d, J = 5.9 Hz, 2H), 4.12 (t, J = 6.6 Hz, 2H), 3.93 (s, 3H), 3.76 (s, 2H), 1.89 (m, 2H), 1.80 (t, J = 5.9 Hz, 1H), 1.65 (m, 2H), 1.43–1.27 (m, 8H), 0.86 (t, J = 6.6 Hz, 3H). ^{13}C NMR (100 MHz, $CDCl_3$) δ = 166.4, 159.3, 142.4, 132.8, 130.8, 130.3, 129.7, 129.2, 126.03, 124.1, 121.3, 117.4, 117.0, 112.2, 94.9, 86.1, 68.7, 63.8, 52.1, 31.6, 29.1, 28.9, 25.8, 23.1, 22.4, 13.9. HRMS-ESI: $C_{54}H_{62}N_2NaO_8$ $[M_2 + Na]^+$, Calculated: 889.4404, Found: 889.4372.

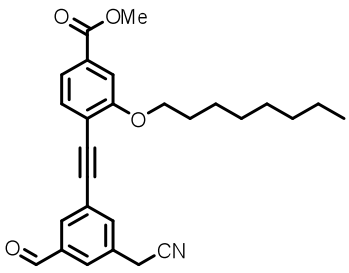

Methyl 4-((3-(cyanomethyl)-5-formylphenyl)ethynyl)-3-(octyloxy)benzoate (5): PCC (920 mg, 4.26 mmol) and silica gel (5 g) were mixed well using a mortar and pestle and suspended in CH_2Cl_2 (50 mL). A solution of methyl 4-((3-(cyanomethyl)-5-(hydroxymethyl)phenyl)ethynyl)-3-(octyloxy)benzoate (1.23 g, 2.84 mmol) in CH_2Cl_2 (30 mL) was dropwise added while stirring. The reaction mixture was stirred at room temperature overnight

and filtered through a short silica gel column and washed with CH_2Cl_2 to give a white solid product (1.08 g, 2.50 mmol, 88% yield). ^{1}H NMR (300 MHz, $CDCl_3$) δ = 10.03 (s, 1H), 7.99 (s, 1H), 7.82 (s, 1H), 7.77 (s, 1H), 7.63 (dd, J = 8.0, 1.4 Hz, 1H), 7.57 (d, J = 1.1 Hz, 1H), 7.54 (d, J = 7.7 Hz, 1H), 4.13 (t, J = 6.6 Hz, 2H), 3.94 (s, 3H), 3.85 (s, 2H), 1.90 (m, 2H), 1.58 (m, 2H), 1.40–1.27 (m, 8H), 0.85 (t, J = 6.6 Hz, 3H). ^{13}C NMR (100 MHz, $CDCl_3$) δ = 190.5, 166.4, 159.7, 137.1, 136.1, 133.1, 132.7, 131.5, 127.9, 125.6, 121.5, 116.7, 116.4, 112.4, 93.3, 88.0, 68.9, 52.3, 31.7, 29.2, 29.0, 26.0, 23.2, 22.6, 14.0. HRMS-EI: $C_{27}H_{29}NO_4$, M^+, Calculated: 431.2091, Found: 431.2094.

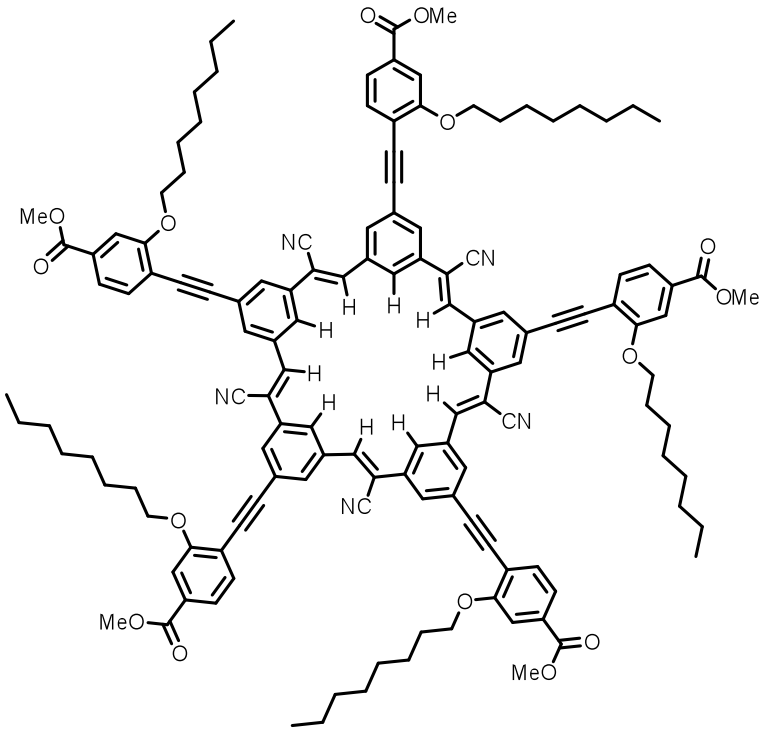

(Methyl 4-ethynyl-3-(octyloxy)benzoate)$_5$-cyanostar (CS-2): To a solution of methyl 4-((3-(cyanomethyl)-5-formylphenyl)ethynyl)-3-(octyloxy)benzoate (100 mg, 0.232 mmol) in THF (12 mL) was added NaOH (2 mg, 0.046 mmol) and NaI (35 mg, 0.23 mmol) in MeOH (12 mL) and stirred overnight at room temperature. Solvents were removed in vacuo. Column chromatography on silica gel with CH_2Cl_2:EtOAc = 9:1 resulted in a yellow solid product (32 mg, 0.015 mmol, 33% yield). ^{1}H NMR (400 MHz, CD_2Cl_2) δ = 8.38 (s, 5H), 7.75 (s, 5H), 7.65 (s, 5H), 7.49–7.40 (m, 15H), 4.04 (t, J = 6.3 Hz, 10H), 3.84 (s, 15H), 1.92 (m, 10H), 1.54 (m, 10H), 1.42 (m, 10H), 1.32–1.24 (m, 40H), 0.80 (t, J = 6.6 Hz, 15H). ^{13}C NMR (125 MHz, $CDCl_3$) δ = 166.3, 159.6, 140.4, 134.1, 133.8, 133.1, 131.9, 131.1, 129.6, 127.8, 126.1, 121.2, 116.6, 116.5, 112.1, 110.6, 94.0, 88.4, 68.9, 52.2, 31.8, 29.34, 29.25, 28.9, 25.9, 22.7, 14.1. HRMS-ESI: $C_{135}H_{135}N_5O_{15}I$ $[M + I]^-$, Calculated: 2193.9033, Found: 2193.9063.

S.8 ^{1}H NMR and ^{13}C NMR Spectroscopy of Compounds

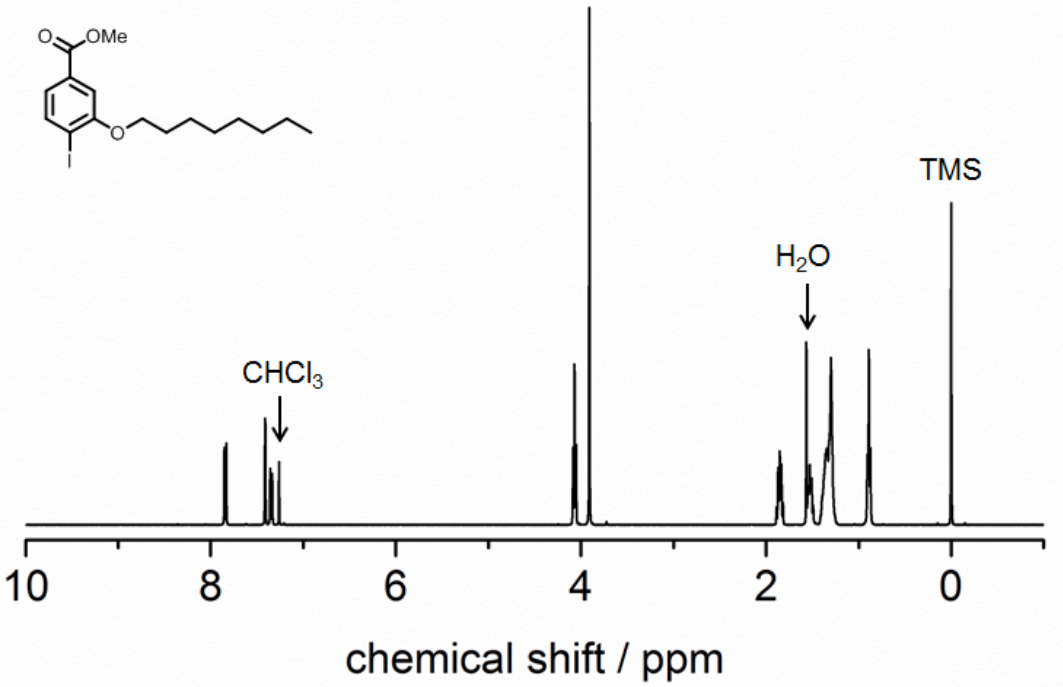

Figure S18. ^{1}H NMR of compound **1**.

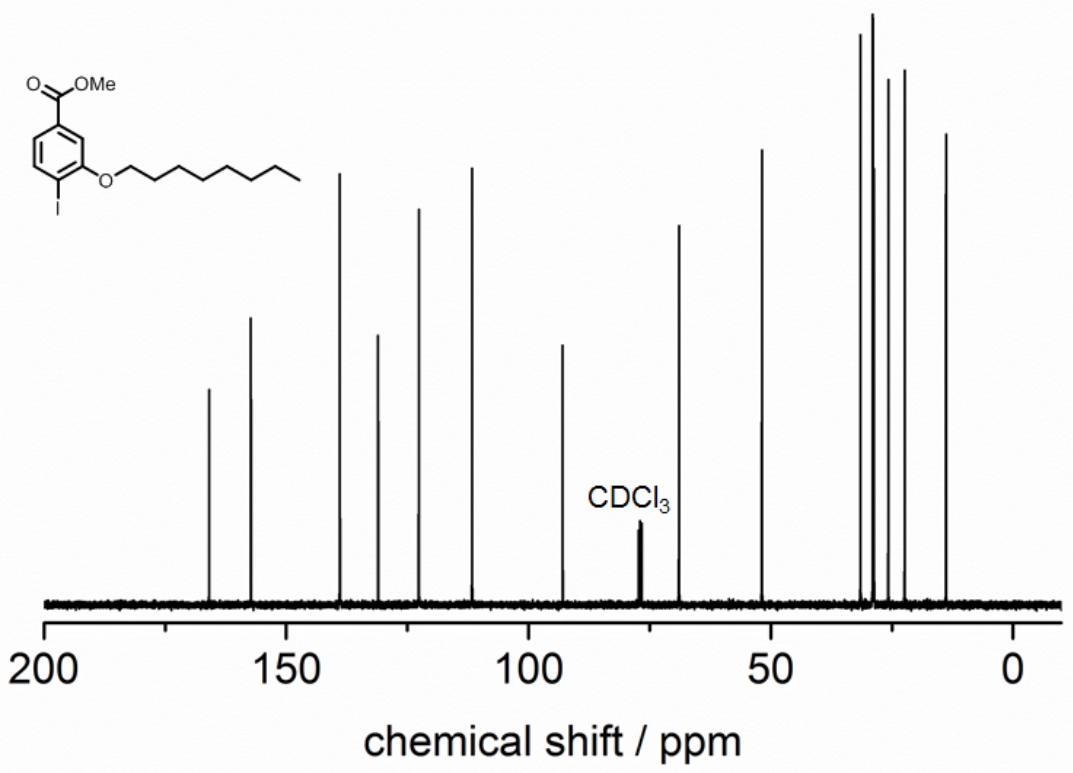

Figure S19. ^{13}C NMR of compound **1**.

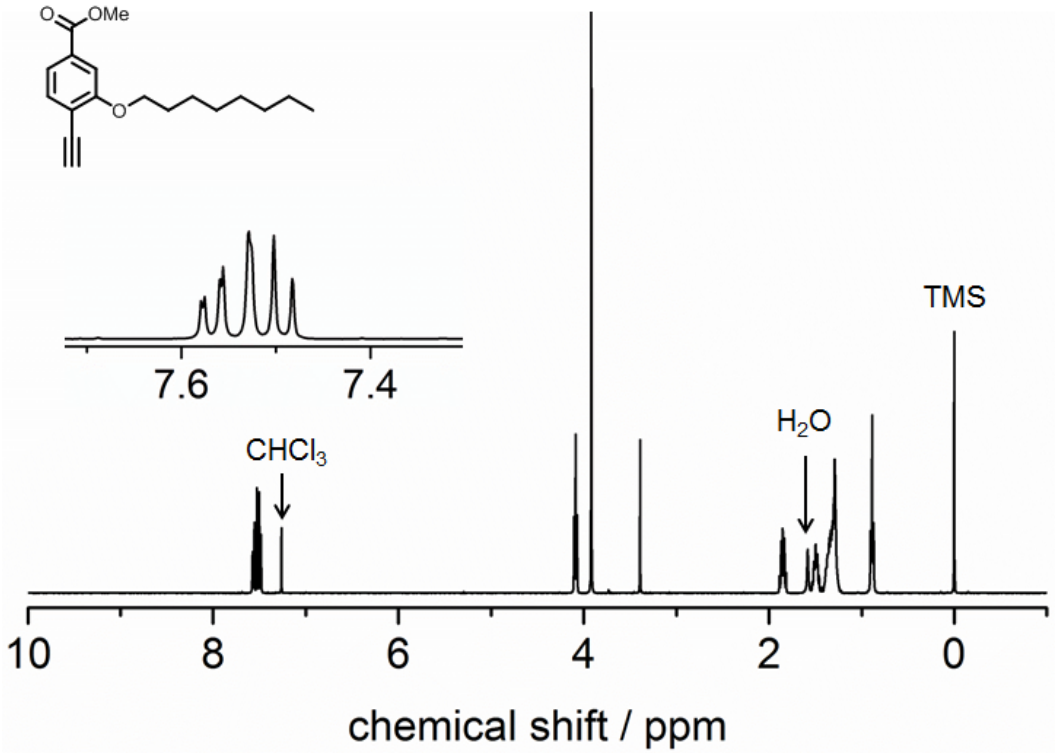

Figure S20. ^{1}H NMR of compound **2**.

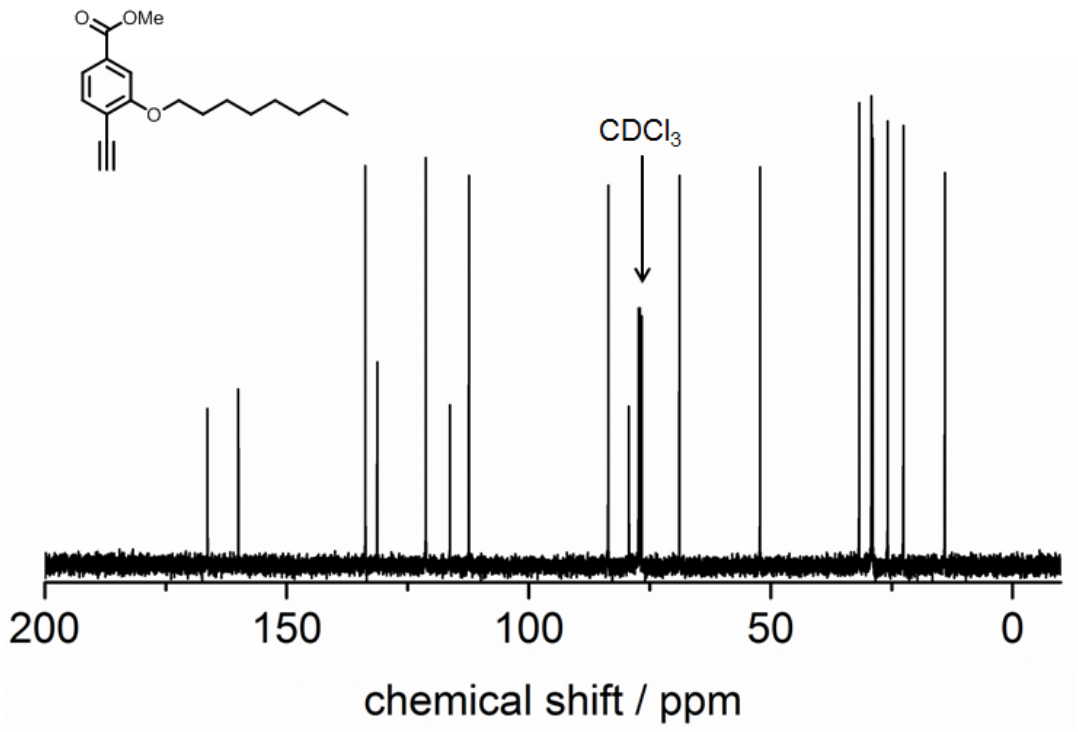

Figure S21. ^{13}C NMR of compound **2**.

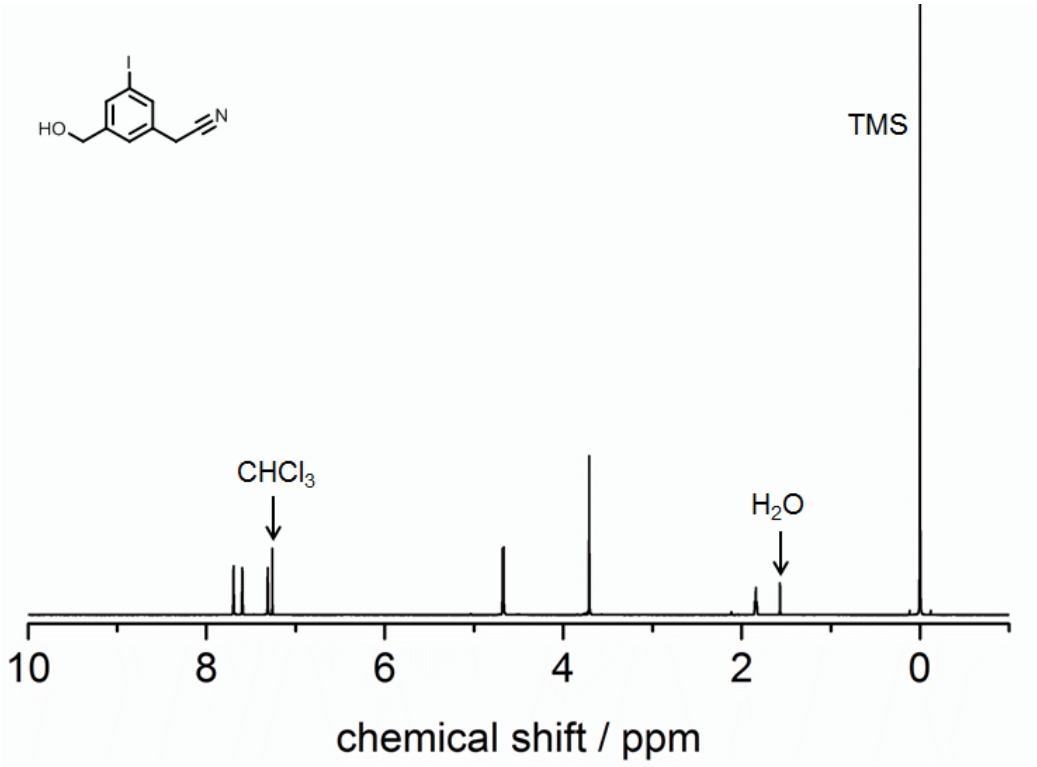

Figure S22. ^{1}H NMR of compound **3**.

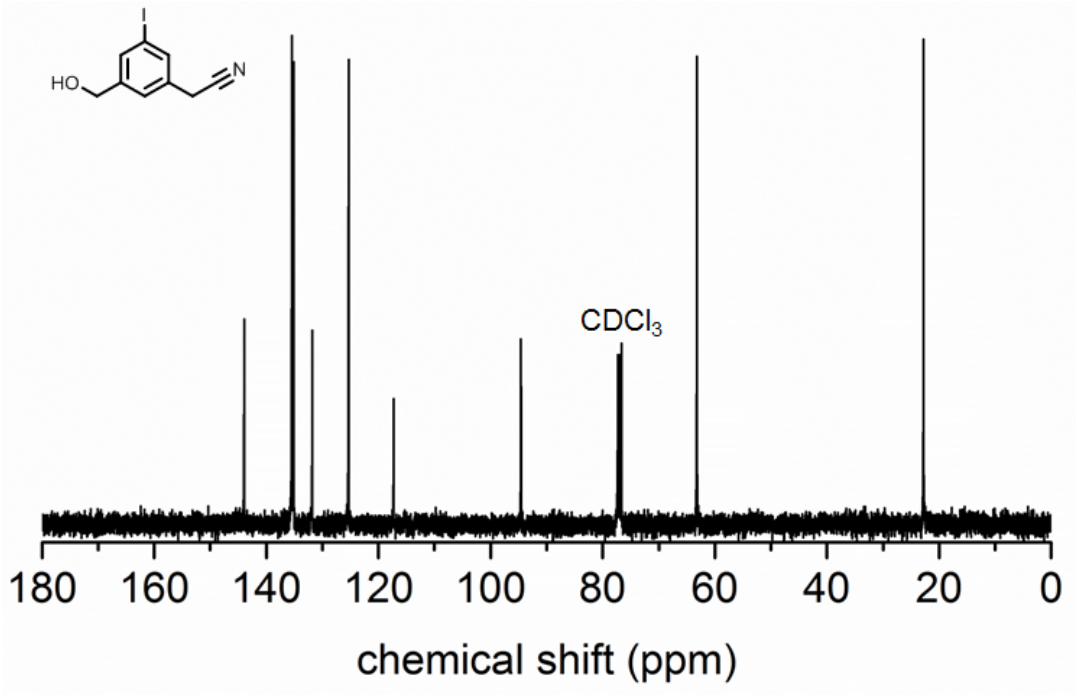

Figure S23. ^{13}C NMR of compound **3**.

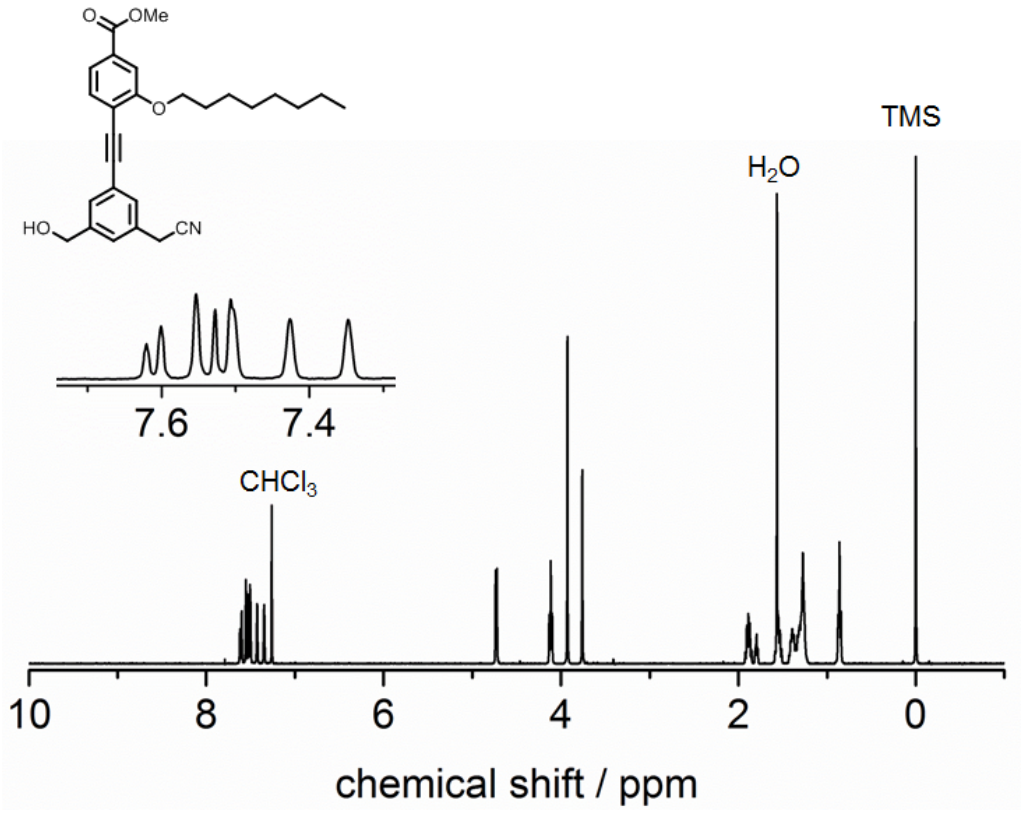

Figure S24. ^{1}H NMR of compound **4**.

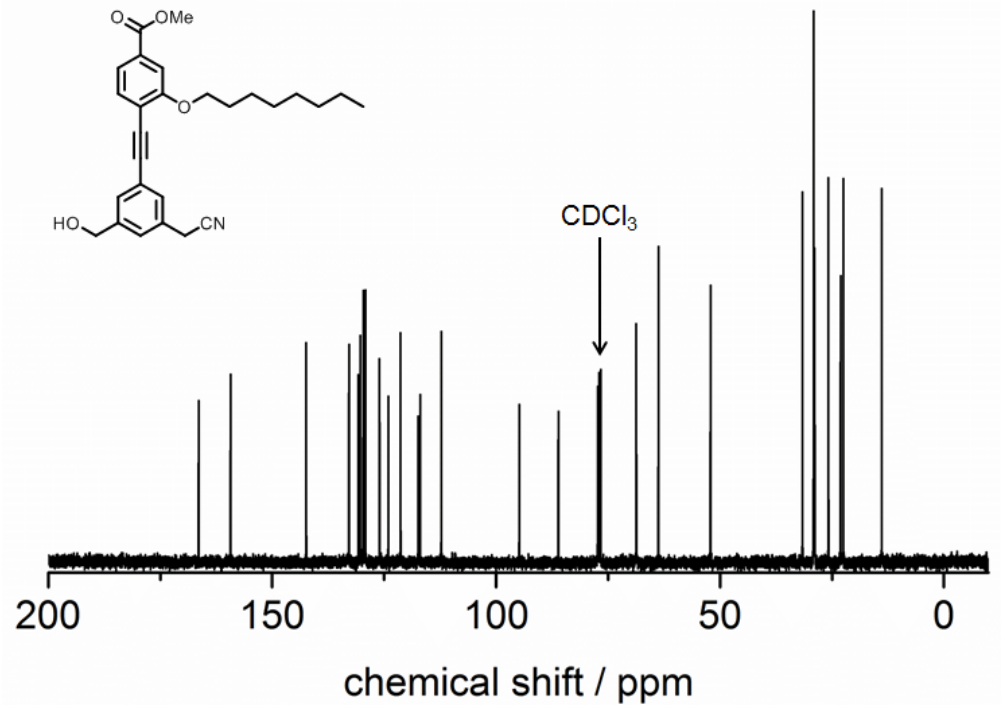

Figure S25. ^{13}C NMR of compound **4**.

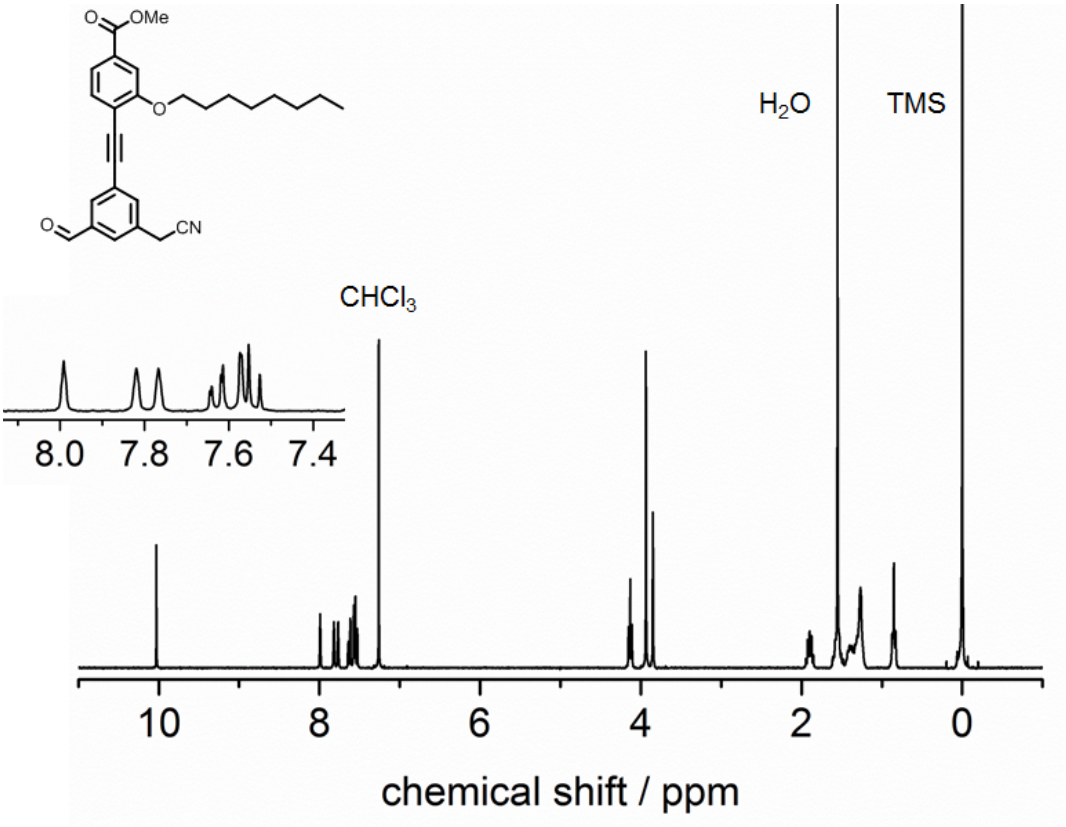

Figure S26. ^{1}H NMR of compound **5**.

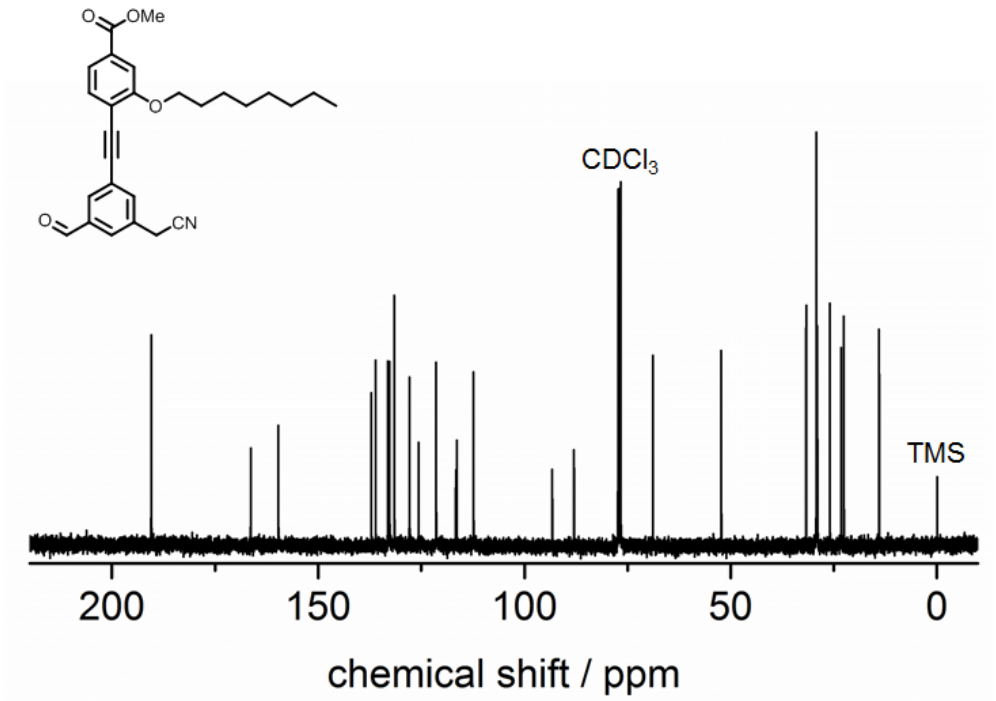

Figure S27. ^{13}C NMR of compound **5**.

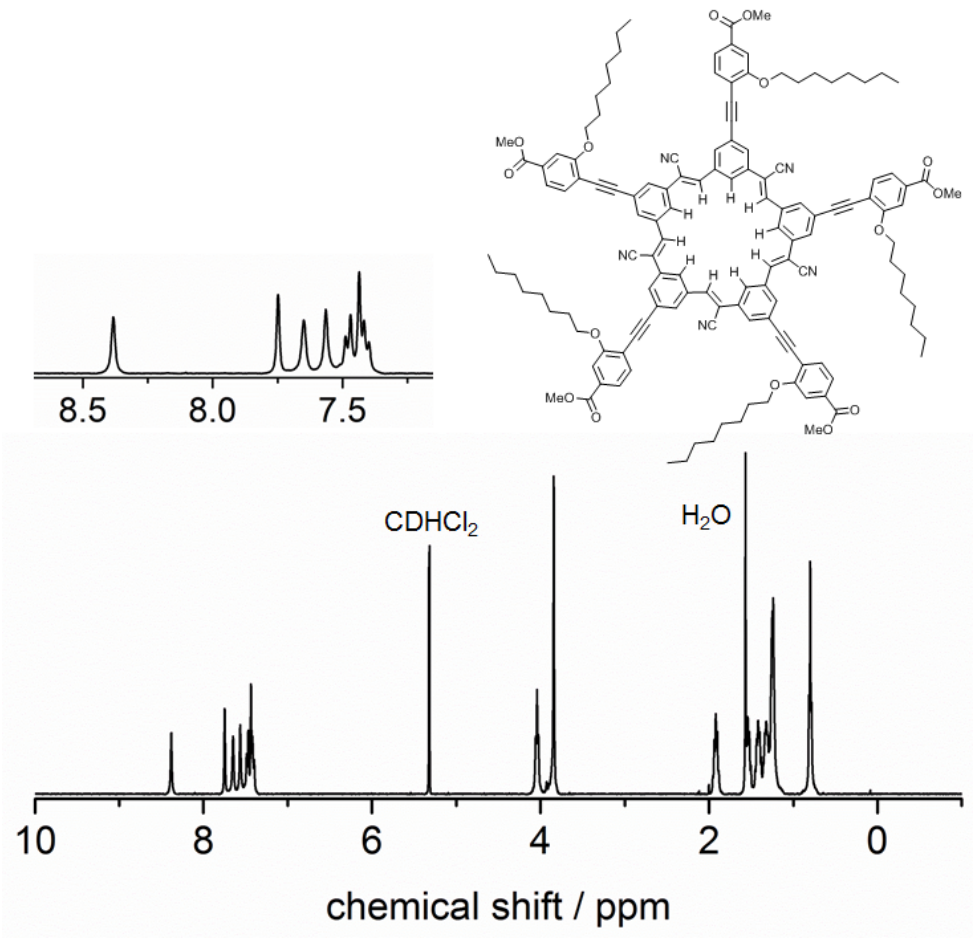

Figure S28. ^{1}H NMR of compound **CS-2**.

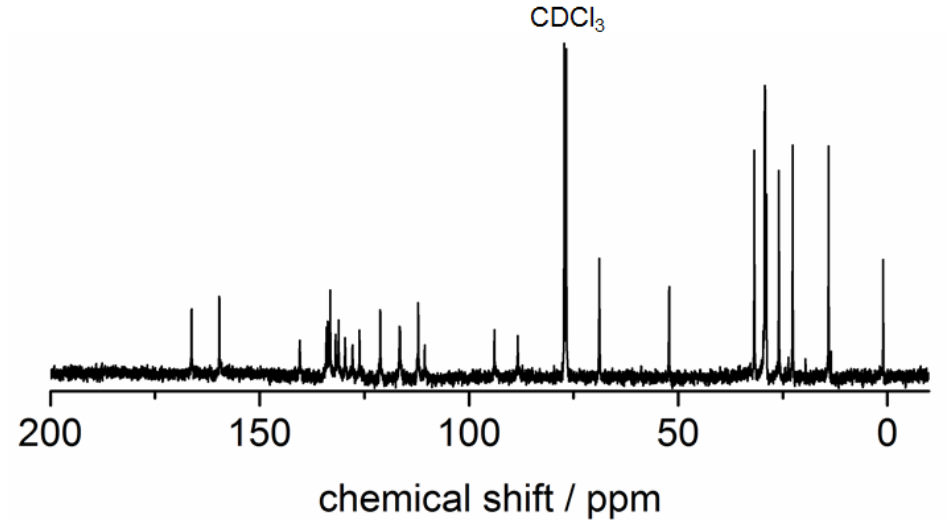

Figure S29. ^{13}C NMR of compound **CS-2**.

References

S1 M. G. Rossmann*, Acta Crystl. Section A,* 1990, **46**, 73

S2 S. Lee, C.-H. Chen and A. H. Flood, *Nat. Chem*., 2013, **5**, 704.

S3 SAINT, Bruker Analytical X-Ray Systems, Madison, WI, current version.

S4 R. Blessing, *Acta Cryst. Section A*, 1995, **51**, 33.

S5 A. Altomare, G. Cascarano, C. Giacovazzo, A. Guagliardi, M. C. Burla, G. Polidori and M. Camalli, *J. Appl. Cryst.*, 1994, **27**, 435.

S6 P. W. Betteridge, J. R. Carruthers, R. I. Cooper, K. Prout and D. J. Watkin, *J. Appl. Cryst.*, 2003, **36**, 1487.

S7 P. van der Sluis and A. L. Spek, *Acta Cryst. Section A*, 1990, **46**, 194.

S8 T. Peterle, P. Ringler and M. Mayor, *Adv. Funct. Mater.*, 2009, **19**, 3497.

S9 (a) A. Speicher, T. Backes, K. Hesidens and J. Kolz, *Beilstein J. Org. Chem.*, 2009, **5**, 71. (b) D. Rankine, A. Avellaneda, M. R. Hill, C. J. Doonan and C. J. Sumby, *Chem. Commun.*, 2012, **48**, 10328.